

Role of Alloyed Sc on the Corrosion Behavior of Mg



PENGYU ZHAO, TIAN XIE, TAO YING, HONG ZHU, and XIAOQIN ZENG

The role of alloyed Sc on the corrosion behavior of Mg was revealed using an understanding of the anodic and cathodic kinetics derived from experimental measurements and DFT calculations. After T4 solution treatment, the Mg–Sc alloy exhibited higher corrosion resistance than high pure Mg. The scandium oxide-rich surface layers formed on the T4 Mg–Sc alloy seemed to suppress anodic dissolution by being protective, and the addition of Sc could inhibit cathodic hydrogen evolution.

<https://doi.org/10.1007/s11661-021-06548-3>

© The Minerals, Metals & Materials Society and ASM International 2021

MAGNESIUM (Mg) alloys are promising candidates for the design of lighter engineering systems,^[1] which are often limited by their high susceptibility to corrosion.^[2] Many researchers^[3] have reported improvements in the corrosion performance of Mg by alloying. Among alloying candidates, rare earth (RE) elements have garnered interest as potential additives for corrosion-resistant Mg alloys.^[4] RE element additives demonstrate many different benefits. For example, the introduction of Y,^[5] Ce,^[6] Nd,^[6] and La^[6] have been shown to reduce the content of iron impurities in Mg, whereas the presence of Sc, Y, La, Ce, Pr, Nd, Sm, Gd, Tb, Dy, Ho, Er, Tm, Yb, and Lu have been proven to form intermetallic compounds with a lower electrode potential.^[7] Furthermore, alloys containing Sc,^[8,9] Y,^[8,10] Ce,^[11] La,^[11] and Nd^[12] have increased the corrosion resistance of the surface layers. Among the RE elements, Sc has a high solid solubility in Mg^[8] and grain refining effect,^[13] and is therefore regarded as an ideal alloying element for Mg alloys. Zhang^[9] studied the corrosion behavior of Mg–Sc binary alloys in a 3.5 wt pct NaCl solution, and attributed their superior performance to the modified microstructure and the formation of protective surface layers. Likewise, Brar^[13] investigated the degradation behavior of Mg–Sc–Y

alloys and demonstrated the effectiveness of Sc to form a self-passivating protective films on the alloys' surface. Previous studies^[8,9,13] have mainly focused on the impact of Sc content on the corrosion performance of Mg. Therefore, the intrinsic mechanism by which Sc affects cathodic and anodic kinetics remains unexplored.

Density functional theory (DFT) calculations have been widely used to determine the reaction mechanisms on material surfaces.^[14] By calculating the hydrogen adsorption energy and the barriers for the hydrogen evolution reaction (HER), the surface conditions for cathodic kinetics can be elucidated.^[14–16] Therefore, the aim of this study is to reveal the underlying mechanism of Sc alloying on Mg corrosion by combining DFT calculations with experimental measurements, such as microstructural characterization, immersion, and electrochemical measurements.

Herein, the binary Mg–4 wt pct Sc (Mg–4.2 wt pct Sc with Fe < 0.015 wt pct, Cu < 0.003 wt pct, Ni < 0.002 wt pct) alloy was prepared using the conventional resistance furnace melting. The detailed melting parameters can be found elsewhere.^[8] The as-cast Mg–Sc alloy was subjected to T4 heat treatment at 450 °C for 36 hours, followed by water quenching. High-purity Mg (referred to hereinafter as HP Mg with Mg > 99.99 wt pct, Fe < 0.005 wt pct, Cu < 0.001 wt pct, Ni < 0.001 wt pct) was used for comparison. The microstructure and corrosion morphology were observed using field-emission scanning electron microscopy (SEM, FEI Sirion 200, in backscattered electron mode) combined with energy-dispersive X-ray spectroscopy (EDS). *In-situ* hydrogen evolution observation was recorded using an optical microscope (OM, Zeiss Axio Observer A1). The phase constituents were identified using X-ray diffraction (XRD, Bruker D8 ADVANCE Da Vinci) with 3 kW CuK α radiation. Scanning Kelvin probe force microscopy (SKPFM, Bruker Dimension Icon & FastScan Bio) was employed to investigate the surface Volta potential fluctuations. The surface layers were analyzed

PENGYU ZHAO, TIAN XIE, and TAO YING are with the National Engineering Research Center of Light Alloy Net Forming, School of Materials Science and Engineering, Shanghai Jiao Tong University, Shanghai, 200240, P.R. China. Contact e-mail: yingtao85@sjtu.edu.cn HONG ZHU is with the University of Michigan - Shanghai Jiao Tong University Joint Institute, Shanghai Jiao Tong University, 200240, Shanghai, P.R. China and also with the State Key Lab of Metal Matrix Composites, Shanghai Jiao Tong University, 200240, Shanghai, P.R. China. XIAOQIN ZENG is with the National Engineering Research Center of Light Alloy Net Forming, School of Materials Science and Engineering, Shanghai Jiao Tong University and also with the State Key Lab of Metal Matrix Composites, Shanghai Jiao Tong University. Contact e-mail: xqzeng@sjtu.edu.cn

Manuscript submitted June 7, 2021; accepted November 10, 2021.

Article published online January 6, 2022

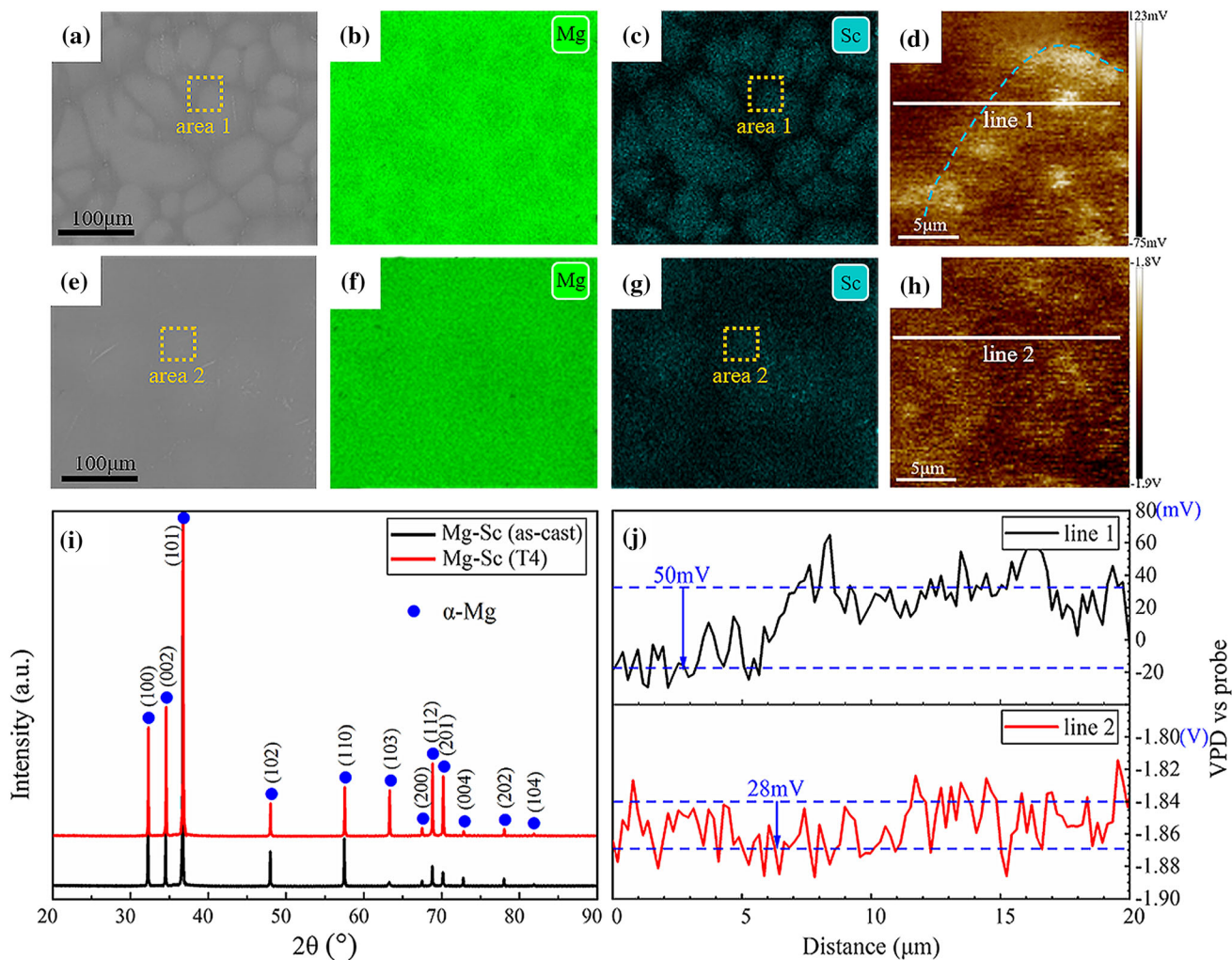


Fig. 1—SEM micrographs (a, e), Mg elemental maps (b, f), Sc elemental maps (c, g), Volta potential maps (d, h) corresponding to the area shown in (c, g) of as-cast Mg–Sc alloy and T4 Mg–Sc alloy, respectively; (i) XRD patterns of the alloys; (j) Potential profiles of line 1 and line 2 shown in (d, h).

using X-ray photoelectron spectroscopy (XPS, Kratos AXIS Ultra DLD) with monochromatic AlK α ray.

The corrosion tests performed were immersion and electrochemical measurements. The specimens were exposed to a 3.5 wt pct NaCl solution at room temperature. Hydrogen evolution and weight loss measurements were performed according to the apparatus and procedure described in Reference 17. Before observing the corrosion morphology, the corrosion products were removed by chemical cleaning according to ASTM G1-03.^[18] Polarization curves were recorded using an Autolab 302N electrochemical workstation with a three-electrode cell (a saturated calomel electrode as the reference electrode, a high-purity platinum filament as the counter electrode, and the specimen as the working electrode).^[8] The open circuit potential (OCP) was monitored for 3600 seconds. Polarization tests were conducted in the anodic and cathodic directions separately at a scan rate of 1 mV/s from the OCP.

DFT calculations were carried out using the Vienna Ab initio Simulation Package (VASP) with the Perdew–Burke–Ernzerhof functional (PBE) and the projector augmented wave (PAW) method.^[19–21] The cutoff energy was set to 480 eV, and $1 \times 1 \times 1$ k-point meshes were used. The electronic convergence threshold was 1×10^{-5} eV. A periodic $5 \times 5 \times 4$ supercell (100 atoms) was constructed to study the hydrogen adsorption with the bottom 2 layers fixed during the calculations. A 15 Å vacuum region was set to prevent interactions between periodic images in all models.^[22] The adsorption energy was calculated using the method described in the previous works.^[23] To calculate the barriers for HER, the Nudged Elastic Band (NEB) method was used following the method introduced in our previous work.^[16] The van der Waals (VDW) interaction was considered using the DFT-D3 method.^[24] The technical details of the models and calculation methods are described in the supplementary material.

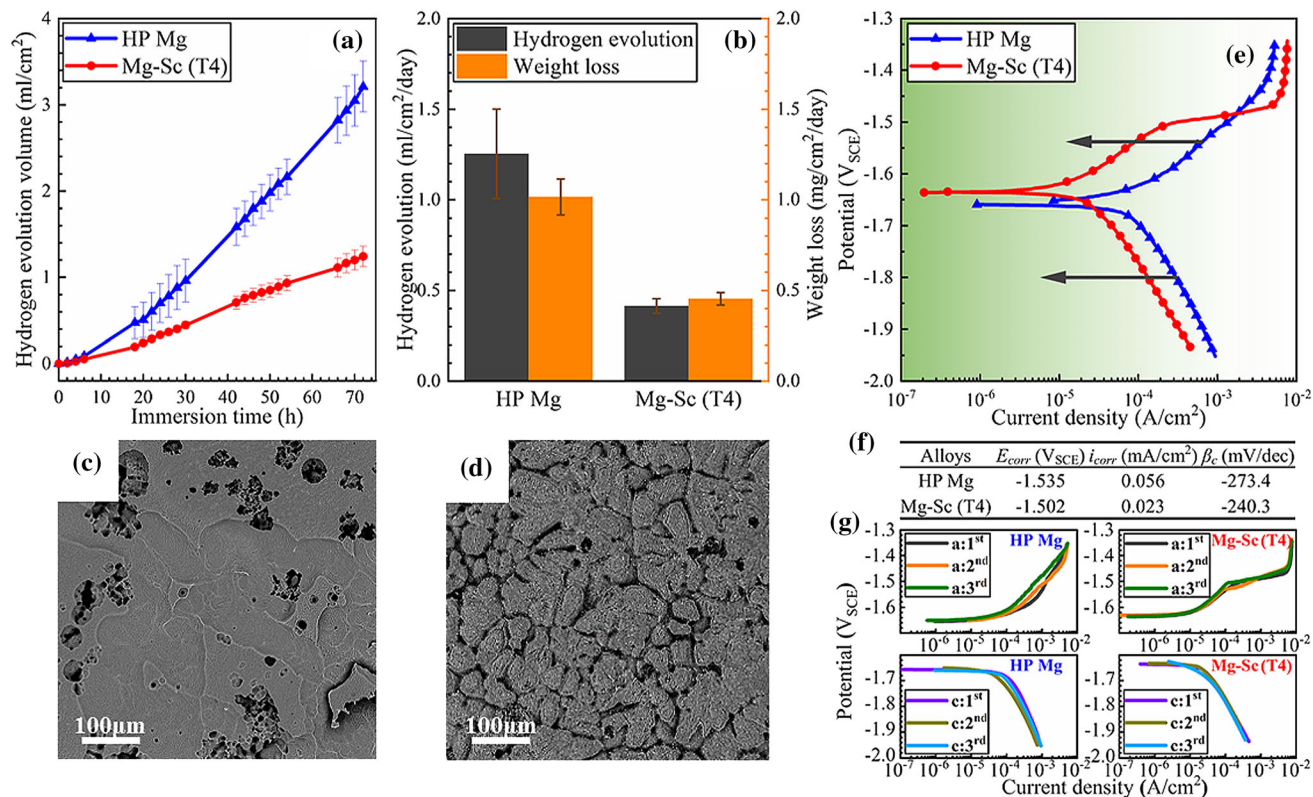


Fig. 2—(a) Hydrogen evolution volume of the investigated alloys during immersion tests for 72h, with the corresponding (b) hydrogen evolution and weight loss rate; (c, d) Corrosion morphology of HP Mg and T4 Mg-Sc alloy immersed for 24 h, respectively; (e) Representative polarization curves of the investigated alloys, with the parameters (f) corrosion potential (E_{corr}), corrosion current density (i_{corr}), and cathodic Tafel slope (β_c); (g) Polarization curves with three replicated measurements, i.e., 1st (the first curve), 2nd (the second curve), and 3rd (the third curve), in the anodic (referred as 'a') and cathodic (referred as 'c') directions separately. The error bars correspond to the standard deviation of multiple measurements.

The as-cast Mg-Sc alloy was subjected to T4 heat treatment. As shown in Figures 1(a) through (h), Mg and Sc were more uniformly distributed in the Mg-Sc alloy after T4 heat treatment (see Figures 1(e) through (h)) compared to the as-cast Mg-Sc alloy (see Figures 1(a) through (d)). This fact is also evident from the Volta potential difference, which decreased from 50 mV in the case of the as-cast Mg-Sc alloy to 28 mV following T4 heat treatment (see Figure 1(j)). Additionally, as the XRD patterns revealed, only α -Mg peaks were resolved, indicating that the investigated alloys were in a single-phase state. Therefore, the single-phase T4 Mg-Sc alloy possesses a uniform potential and distribution of elements, which can be used to better understand the role alloyed Sc plays in the corrosion behavior of Mg.

The corrosion behavior was investigated using the corrosion tests shown in Figure 2. For the HP Mg and T4 Mg-Sc alloys, the evolved H₂ volumes increased linearly with immersion time. However, the hydrogen evolution rate of T4 Mg-Sc alloy (0.41 ml/cm²/day) was lower than that of HP Mg (1.02 mL/cm²/day). Likewise, the T4 Mg-Sc alloy had a smaller hydrogen evolution rate compared to the value reported for the Mg-0.3 wt pct Sc alloy by Zhang.^[9] As shown in Figures 2(c) and (d), HP Mg exhibits a localized corrosion morphology. The T4 Mg-Sc alloy generally undergoes uniform

corrosion within the Sc distribution regions, despite the inhomogeneous corrosion morphology caused by fluctuations of the Sc distribution.^[8] The rankings of the corrosion current density (i_{corr}) (see Figure 2(f)) are consistent with the immersion results shown in Figure 2(b). To elucidate the corrosion behavior, the anodic and cathodic polarization curves were recorded separately and are presented in Figure 2(e). Regarding the anodic branch, the T4 Mg-Sc alloy exhibits a decreased anodic current density, which is related to the inhibited anodic dissolution. In terms of the cathodic branch that is associated with the HER, the cathodic current density decreases in the T4 Mg-Sc alloy, indicating depressed H₂ evolution kinetics.

To reveal the underlying mechanism behind Sc's effect on Mg corrosion, cathodic and anodic kinetics were discussed separately. In the corrosion process of Mg alloys, the HER plays a determining role in the cathodic kinetics.^[15,23] The HER in a neutral or base solution can be discussed in the following steps: the adsorption of H atoms, the combination of two nearby H atoms, and the release of H₂ gas.^[16] As depicted in Figure 3(a), the Mg (0001) surface with a one Sc atom replacement is denoted as the Mg-Sc surface. First, the H atom adsorption energy at different sites on the Mg surface, as well as on the Mg-Sc surface, was calculated. As shown in Figure 3(b), the H atom adsorption energy on

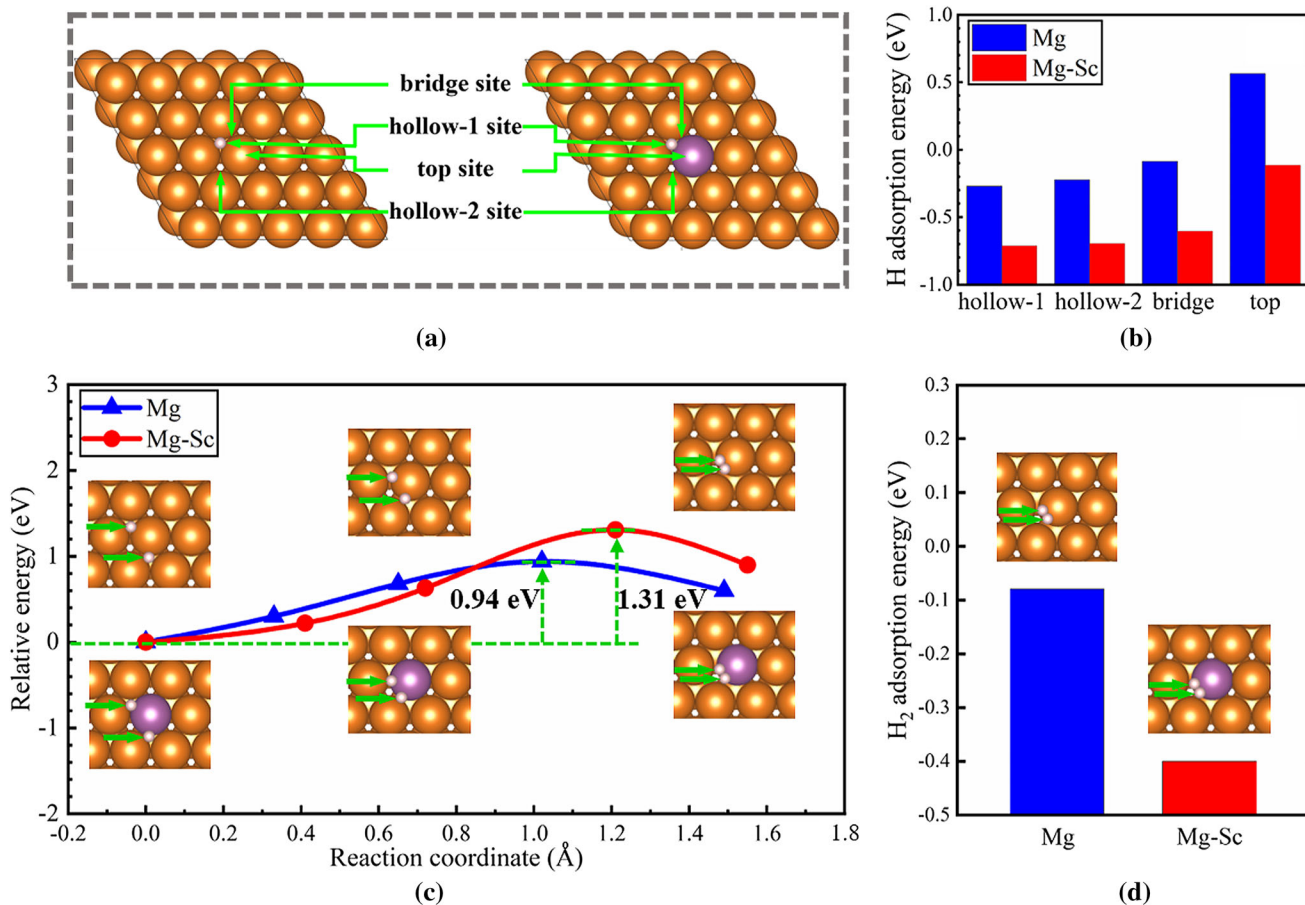


Fig. 3—(a) Representative bridge site, hollow-1 site, top site, and hollow-2 site of the Mg surface or Mg–Sc surface, with the corresponding (b) H atom adsorption energy; (c) Diffusing path and energy barrier of combining two nearby H atoms; (d) H₂ adsorption energy of the final state (c) on Mg surface and Mg–Sc surface. The atoms are colored by type: Mg (brown), Sc (purple). The sites and H atoms are marked with the green arrow (Color figure online).

the Mg–Sc surface is always lower than that on the Mg surface, indicating a stronger tendency to capture H atoms. Subsequently, the H atoms diffused on the surface and combine into H₂ molecules. The energy barriers for the combination of two nearby H atoms on the surfaces were analyzed using the NEB method. As shown in Figure 3(c), the Mg–Sc surface possesses a larger energy barrier, suggesting H atom combination inhibition. Finally, the release of H₂ formed on the surface was investigated by calculating the H₂ adsorption energy. The Mg–Sc surface exhibits a lower H₂ adsorption energy, indicating the stable adsorption of H₂ gas. According to the Sabatier principle,^[23] the HER rate would slow down in the case of a more negative hydrogen adsorption energy, which is attributed to the enhanced H adsorption strength. Therefore, with the addition of Sc, the HER of Mg–Sc alloy would be suppressed.

In-situ hydrogen evolution observations and surface layer analyses were conducted to further reveal the corrosion behavior of Sc alloying. Representative *in-situ* observations are shown in Figures 4(a) through (f). Generally, two types of H₂ bubbles evolve on the surfaces: fine stream bubbles (marked with the yellow

arrows) and spherical bubbles (marked with the pink arrows). Regarding the HP Mg, the evolved H₂ bubbles mostly appear as fine stream bubbles and growing sphere bubbles, which originate from local cathodic sites on impurities.^[25,26] In terms of the T4 Mg–Sc alloy, the bubbles were predominantly stable. No continuous evolution and growth of the H₂ bubbles were observed during the immersion. Therefore, the T4 Mg–Sc alloy exhibits a slower H₂ evolution rate than HP Mg, owing to the lower H atom adsorption energy and larger energy barrier of the H atom combination. In addition, the size of the bubbles that evolved on the T4 Mg–Sc alloy remained almost unchanged, resulting from the enhanced H₂ atom adsorption energy. The hydrogen evolution behavior was consistent with the calculation results, thereby verifying the ability of HER suppression on Mg via Sc alloying.

The anodic dissolution kinetics were analyzed from the viewpoint of the surface layers. As shown in Figure 4(g), Sc₂O₃ was found in the surface layers of the T4 Mg–Sc alloy. According to a previous study,^[8] the presence of Sc₂O₃ (Pilling–Bedworth ratio > 1) can improve the coverage integrity and protectiveness of the Mg surface layers, thereby rendering the dissolution of

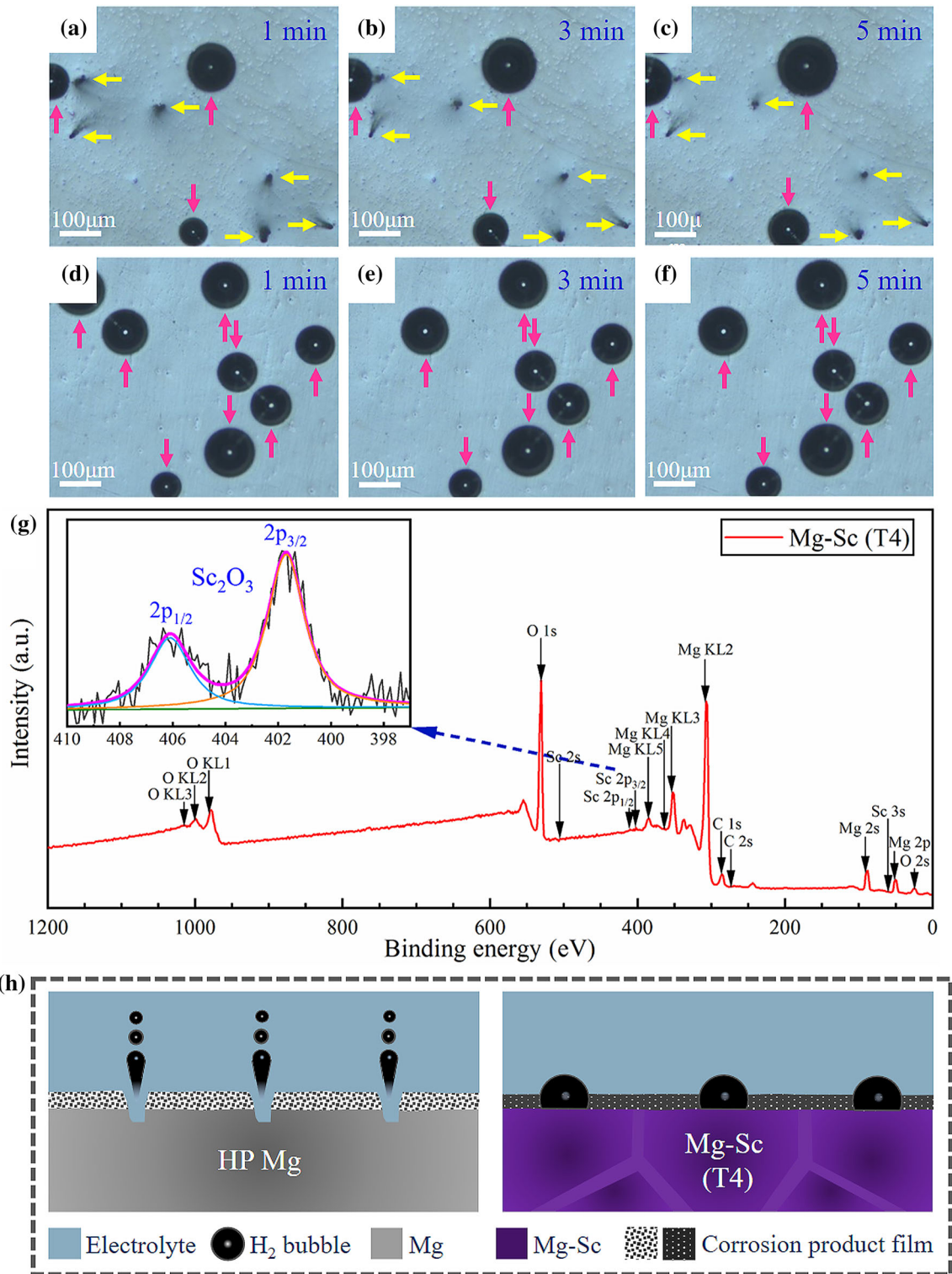


Fig. 4—Representative *in-situ* hydrogen evolution observation on HP Mg (a to c) and T4 Mg-Sc (d, to f) immersed for 1, 3, and 5 min respectively; (g) XPS profiles of T4 Mg-Sc alloy surface after immersion for 1 h, with the inset for narrow scan of Sc 2p spectra; (h) Depiction of corrosion mechanism on HP Mg and T4 Mg-Sc alloy.

the Mg matrix, which explains the decreased anodic current density in the polarization curves (see Figure 3(e)). Therefore, more protective surface layers could be provided with Sc alloying, which is consistent with the results reported by Zhan.^[9]

In summary, the role of alloyed Sc on the corrosion behavior of Mg was revealed using both the experimental measurements and DFT calculations. In the case of Sc alloying, the scandium oxide-rich surface layers formed on the T4 Mg-Sc alloy appeared to suppress

the anodic dissolution by being protective. Additionally, alloyed Sc inhibits the HER by enhancing the adsorption of H atoms, impeding the combination of H atoms and the release of H₂ gas as shown by DFT calculations. As depicted in Figure 4(h), owing to the suppressed anodic and cathodic kinetics, the T4 Mg–Sc alloy exhibits higher corrosion resistance than HP Mg after T4 heat treatment.

This work was supported by National key research and development program (No. 2020YFB1505901), Science and Technology Commission of the CMC (2019JCJQZD27300), Foundation from Shanghai Jiao Tong University (AF0500132, AF0500149), and Funding from Center of Hydrogen Science of Shanghai Jiao Tong University. Thanks for the technology support from Instrumental Analysis Center, Shanghai Jiao Tong University.

On behalf of all authors, the corresponding author states that there is no conflict of interest.

SUPPLEMENTARY INFORMATION

The online version contains supplementary material available at <https://doi.org/10.1007/s11661-021-06548-3>.

REFERENCES

1. Z. Wu, R. Ahmad, B. Yin, S. Sandlöbes, and W.A. Curtin: *Science*, 2018, vol. 359, pp. 447–52.
2. M. Esmaily, J.E. Svensson, S. Fajardo, N. Birbilis, G.S. Frankel, S. Virtanen, R. Arrabal, S. Thomas, and L.G. Johansson: *Prog. Mater. Sci.*, 2017, vol. 89, pp. 92–193.
3. A. Atrens, Z. Shi, S.U. Mehreen, S. Johnston, G.L. Song, X. Chen, and F. Pan: *J. Magn. Alloy*, 2020, vol. 8, pp. 989–98.
4. H. Azzeddine, A. Hanna, A. Dakhouche, L. Rabahi, N. Scharnagl, M. Dopita, F. Brisset, A.L. Helbert, and T. Baudin: *J. Alloys Compd.*, 2020, vol. 829, p. 154569.

5. J. Il, H. Ngoc, B. Sun, and Y. Min: *Scr. Mater.*, 2019, vol. 162, pp. 355–60.
6. S. Zhu, Z. Liu, R. Qu, L. Wang, Q. Li, and S. Guan: *J. Magn. Alloy*, 2013, vol. 1, pp. 249–55.
7. J. Meng, W. Sun, Z. Tian, X. Qiu, and D. Zhang: *Corrosion Performance of Magnesium (Mg) Alloys Containing Rare-Earth (RE) Elements*, Woodhead Publishing Limited, Swaston, 2013.
8. P. Zhao, T. Xie, X. Xu, H. Zhu, F. Cao, T. Ying, and X. Zeng: *Metall. Mater. Trans. A*, 2020, vol. 51A, pp. 2509–22.
9. C. Zhang, L. Wu, H. Liu, G. Huang, B. Jiang, A. Atrens, and F. Pan: *Corros. Sci.*, 2020, vol. 174, p. 108831.
10. M. Liu, P. Schmutz, P.J. Uggowitzer, G. Song, and A. Atrens: *Corros. Sci.*, 2010, vol. 52, pp. 3687–3701.
11. W. Liu, F. Cao, L. Chang, Z. Zhang, and J. Zhang: *Corros. Sci.*, 2009, vol. 51, pp. 1334–43.
12. R. Arrabal, A. Pardo, M.C. Merino, M. Mohedano, P. Casajús, K. Paucar, and G. Garcés: *Corros. Sci.*, 2012, vol. 55, pp. 301–12.
13. H.S. Brar, J.P. Ball, I.S. Berglund, J.B. Allen, and M.V. Manuel: *Acta Biomater.*, 2013, vol. 9, pp. 5331–40.
14. H. Ke and C.D. Taylor: *Corrosion*, 2019, vol. 75, pp. 708–26.
15. Z. Luo, H. Zhu, T. Ying, D. Li, and X. Zeng: *Surf. Sci.*, 2018, vols. 672–3, pp. 68–74.
16. Z. Luo, J. Xu, Y. Wang, T. Xie, H. Zhu, T. Ying, D. Li, L. Wang, X. Zeng, C. Wolverton, and W. Ding: *J. Electrochem. Soc.*, 2019, vol. 166, pp. C421–27.
17. G. Song, A. Atrens, and D. Suohn: *Essent. Read. Magn. Technol.*, 2014, vol. 9781118858, pp. 565–72.
18. ASTM G1–03 Standard Practice for Preparing, Cleaning and Evaluating Corrosion Test Specimens.
19. G. Kresse and J. Hafner: *Phys. Rev. B*, 1993, vol. 47, pp. 558–61.
20. J.P. Perdew, K. Burke, and M. Ernzerhof: *Phys. Rev. Lett.*, 1996, vol. 50, pp. 308–10.
21. P.E. Blöchl: *Phys. Rev. B*, 1994, vol. 50, pp. 17953–79.
22. N.E. Singh-Miller and N. Marzari: *Phys. Rev. B*, 2009, vol. 80, p. 235407.
23. M. Zhang, L.G. Hector, Y. Guo, M. Liu, and L. Qi: *Comput. Mater. Sci.*, 2019, vol. 165, pp. 154–66.
24. S. Grimme, J. Antony, S. Ehrlich, and H. Krieg: *J. Chem. Phys.*, 2010, vol. 132, p. 154104.
25. A. Yamamoto, A. Watanabe, K. Sugahara, S. Fukumoto, and H. Tsubakino: *Mater. Trans.*, 2001, vol. 42, pp. 1237–42.
26. P.W. Chu, E. Le Mire, and E.A. Marquis: *Corros. Sci.*, 2017, vol. 128, pp. 253–64.

Publisher's Note Springer Nature remains neutral with regard to jurisdictional claims in published maps and institutional affiliations.